

The effects of blade-pitch control on the performance of semi-submersible-type floating offshore wind turbines

H.C. Kim and M.H. Kim*

Texas A&M University, Dept. Ocean Engineering, College Station, TX 77843, USA

(Received December 2, 2017, Revised February 11, 2018, Accepted February 19, 2018)

Abstract. The effects of BPC (blade pitch control) on FOWT (floating offshore wind turbine) motions and generated power are investigated by using a fully-coupled turbine-floater-mooring simulation program. In this regard, two example FOWTs, OC4-5MW semi-submersible FOWT and KRISO four-3MW-units FOWT, are selected since the numerical simulations of those two FOWTs have been verified against experiments in authors' previous studies. Various simulations are performed changing BPC natural frequency (BPCNF), BPC damping ratio (BPCDR), and wind speeds. Through the numerical simulations, it was demonstrated that negative damping can happen for platform pitch motions and its influences are affected by BPCNF, BPCDR, and wind speeds. If BPCNF is significantly larger than platform-pitch natural frequency, the pitch resonance can be very serious due to the BPC-induced negative-damping effects, which should be avoided in the FOWT design. If wind speed is significantly higher than the rated wind velocity, the negative damping effects start to become reduced. Other important findings are also given through systematic sensitivity investigations.

Keywords: FOWT (floating offshore wind turbine); BPC (blade pitch control); BPCNF; BPCDR; negative pitch damping; wind speed; generated power; thrust; fully-coupled turbine-floater-mooring simulation

1. Introduction

Nowadays, more FOWTs (floating offshore wind turbines) are considered and installed in several countries. FOWTs are attractive due to stronger and steadier winds and less regulations in deep waters. More than five full-scale FOWTs have successfully been operated and it is now known to be a proven technology although several details still need to be developed and improved.

For large-size floating wind turbines, the blade-pitch-control (BPC) effects on floater performance need to be investigated in the design stage. The two important BPC parameters are BPC damping ratio (BPCDR) and BPC natural frequency (BPCNF). It is known that when improper values of BPCNF and BPCDR are used, there are harmful (negative-damping) effects on platform motions and generated power. Thus, the adequate BPCNF and BPCDR values have to be selected as changing the PID gain values.

*Corresponding author, Professor, E-mail: m-kim3@tamu.edu

Regarding the negative damping and excessive resonance caused by BPC, Larson and Hanson introduced the stability problem (Larsen and Hanson 2007). Jonkman (2008) performed the BPCNF sensitivity test for barge-type floating base and mentioned that 0.4 rad/sec BPCNF is preferred considering the platform pitch motion. However, there is no warrant that the suggested number also works for other types of FOWT. Namik and Stol (2011) illustrated the effects of the platform motions on various BPC strategies for barge-, TLP-, and spar-type floating bases. However, in above studies, FAST v7.00 was used for the simulations, and the hydro-dynamic forces, mooring dynamics, and coupling between hull and mooring lines were not rigorously calculated without considering full coupling and nonlinear effects. It's important to calculate those contributions and related coupling accurately to better understand the novel effects of BPC on platform motions and generated power.

In our previous works on the global performances of OC4-5 MW semi-submersible FOWT and KRISO MUFOWT(multi-unit FOWT), the platform motions have reliably been simulated and the numerical results were verified against DeepCWind and KRISO experiments (Kim and Kim 2015, 2016, Kim *et al.* 2017). In the numerical simulations, the complete 2nd-order difference-frequency diffraction/radiation wave forces (Kim and Yue 1989, 1990, 1991) and the Morison forces at platform's instantaneous positions in irregular waves were included and the numerical results agreed well with experimental results. Since the simulations of those two FOWTs were verified against experiments, we use the same numerical tool for further investigating the effects of BPC strategies on the global performances of the respective platforms and the resulting power outputs.

The fully-coupled dynamic-analysis tool CHARM3D-FAST, the combination of FAST (e.g., Jonkman and Buhl 2005) developed by NREL and CHARM3D (e.g., Yang and Kim 2010, 2011) has been developed by the second author's research group (e.g., Bae and Kim 2011). The program was further extended to be able to simulate multiple wind turbines on a single floater (Bae and Kim 2014). The full dynamic approach of mooring line is employed using finite element method (FEM) instead of quasi-static approach. More rigorous wave kinematics near MWL were implemented for evaluating viscous drag forces on Morison members up to the instantaneous free-surface elevation. The best drag coefficients were selected based on the comparison study between model tests and numerical simulations.

In this paper, systematic sensitivity tests with BPC parameters and wind speeds are performed for the KRISO MUFOWT and OC4 semi-submersible FOWT using the FAST-CHARM3D. The pitch natural frequencies of the two platforms are 0.4 rad/s and 0.23 rad/s, respectively. Based on the simulation results, the optimal values of BPCNF and BPCDR are suggested and the related physics are explained. The results will be useful to decide the appropriate gain values for reducing platform motions and satisfy the regulating ability at the same time. The deduced BPC strategy is compared with those of previously published papers (Hansen *et al.* 2005, Jonkman *et al.* 2009, Larsen and Hanson 2007)

2. Torque/blade pitch control

For typical wind turbines, two power control systems are designed to work. A generator-torque controller works for below-rated-wind-speed range and a blade-pitch controller functions in above-rated-wind-speed region. The generator-torque controller is designed to maximize power capture and the blade-pitch controller is intended to regulate power output by gain-scheduled

proportional-integral (PI) control. The schematic diagram of the two control strategies is depicted in Fig. 1.

The controllers determine their feedback order, such as generator torque or blade-pitch angle, by measuring the filtered shaft speed. The measured shaft speed is then compared with the target shaft speed. The error between measured and target shaft speed can be expressed as the equation of motion for the rotor-speed error as shown in Eq. (1), which is obtained from Eqs. (2) and (3).

$$\begin{aligned} & \left[I_{Drivetrain} + \frac{1}{\Omega_0} \left(-\frac{\partial P}{\partial \theta} \right) N_{Gear} K_d \right] \ddot{\varphi} + \left[\frac{1}{\Omega_0} \left(-\frac{\partial P}{\partial \theta} \right) N_{Gear} K_p - \frac{P_0}{\Omega_0^2} \right] \dot{\varphi} + \left[\frac{1}{\Omega_0} \left(-\frac{\partial P}{\partial \theta} \right) N_{Gear} K_i \right] \varphi \\ & = M_\varphi \ddot{\varphi} + C_\varphi \dot{\varphi} + K_\varphi \varphi \\ & = 0 \end{aligned} \tag{1}$$

$$T_{Aero} - N_{Gear} T_{Gen} = (I_{Rotor} + N_{Gear}^2 I_{Gen}) \frac{d}{dt} (\Omega_0 + \Delta\Omega) = I_{Drivetrain} \Delta \dot{\Omega} \tag{2}$$

$$\Delta\theta = K_P N_{Gear} \Delta\Omega + K_I \int_0^t N_{Gear} \Delta\Omega dt + K_D N_{Gear} \Delta \dot{\Omega} \tag{3}$$

Proportional and integral gains are decided from Eqs. (4)-(6)

$$K_p(\theta) = \frac{2I_{Drivetrain} \Omega_0 \zeta_\varphi \omega_{pn}}{N_{Gear} \left[-\frac{\partial P}{\partial \theta}(\theta=0) \right]} GK(\theta) \tag{4}$$

$$K_I(\theta) = \frac{I_{Drivetrain} \Omega_0 \omega_{pn}^2}{N_{Gear} \left[-\frac{\partial P}{\partial \theta}(\theta=0) \right]} GK(\theta) \tag{5}$$

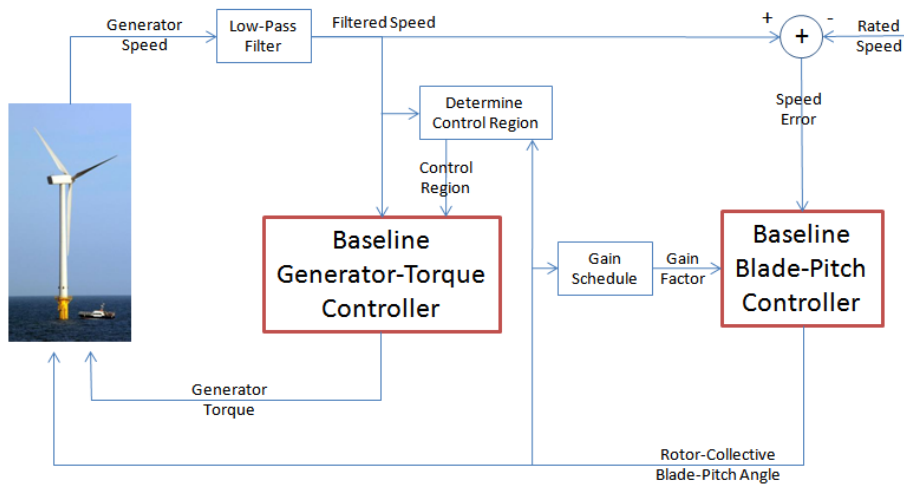


Fig. 1 Two power control strategies

$$GK(\theta) = \frac{I}{I + \frac{\theta}{\theta_k}} \quad (6)$$

The natural frequency, damping ratio, and damped natural frequency are given by Eqs. (7)-(9)

$$\omega_{\varphi n} = \sqrt{\frac{K_{\varphi}}{M_{\varphi}}} \quad (7)$$

$$\zeta_{\varphi} = \frac{C_{\varphi}}{2\sqrt{K_{\varphi}M_{\varphi}}} = \frac{C_{\varphi}}{2M_{\varphi}\omega_{\varphi n}} \quad (8)$$

$$\omega_d = \omega_{\varphi n} \sqrt{1 - \zeta_{\varphi}^2} \quad (9)$$

In Eqs. (1)-(9), $I_{Drivetrain}$ is a drivetrain inertia and P and P_0 are mechanical power and rated mechanical power respectively. θ is a full-span rotor-collective blade-pitch angle and Ω_0 is a rated low-speed shaft rotational speed. $\partial P/\partial \theta$ stands for the sensitivity of aerodynamic power to rotor-collective blade pitch. K_d , K_p , and K_I are the blade-pitch controller proportional, integral, and derivative gains respectively. N_{gear} is gear box ratio. T_{Aero} and T_{Gen} are aerodynamic torque and generator torque respectively.

In Table 1, the properties about blade pitch control of KRISO 3 MW and NREL OC4 5 MW wind turbines are given. The same PI gain values as the OC3 Hywind spar wind-turbine are used (Jonkman 2010). More details about the torque/blade-pitch control are given in NREL report (Jonkman *et al.* 2009). The natural frequency of the blade pitch control system changes according to the blade pitch angle because the K_p and K_I vary with the blade pitch angle based on Eqs. (4)-(6). In the present case, K_d is zero, θ_k is the blade-pitch angle at which the pitch sensitivity has doubled from its value at the rated point, and θ_k of NREL 5MW and KRISO 3 MW wind turbines are 6.30 deg and 2.19 deg respectively. They are estimated by using linear extrapolation from the values in Fig. 2. If the blade pitch angle increases, the integral gain decreases, and it is connected to the decreases of stiffness and the damped natural frequency of blade control system based on the K_p and K_I equations and governing equation. For example, when the natural frequency is 0.2 rad/sec in zero blade pitch angle, if the blade pitch angle increases to 9.0 deg, then the modified natural frequency is 0.128 rad/sec. The damped natural frequencies will decrease more when considering the large damping of the blade pitch control.

To keep the rated power constant, the BPC starts to work in the higher wind speed than the rated wind speed. The blade pitch angle according to the wind speed at hub is decided based on the blade properties, such as, blade shape, twist, and chord. The rotor speed filtered using low-pass filter is estimated and the rotor speed error between the filtered rotor speed and target rotor speed is obtained. Then the rotor speed error is applied to its equation of motion. The equation is derived from the equation of drivetrain motion and the equation of PID control. $\partial P/\partial \theta$ in the Eq. (1) means the sensitivity of the power to the blade pitch (BP) and it is function of BP. This value is calculated through FAST linearization when the wind speed and the BP according to the wind speed are given. The sensitivities of power to pitch of KRISO 3MW wind turbine are shown in Fig. 2. The similar figure for NREL 5MW wind turbine is given in NREL report (Jonkman *et al.* 2009). They are summarized in Table 2. The first order trend equation can be obtained from the points. The equation is applied to the controller and the change of the power sensitivity according to the BP is

considered. Blade pitch control damping ratio (BPCDR) and Blade pitch control natural frequency (BPCNF) can be calculated from Eqs. (7) and (8), respectively. In addition, K_P and K_I are the functions of blade pitch angle, thus the natural frequency and damping ratio change according to the blade pitch angle.

Table 1 Blade pitch control system properties of NREL OC4 5 MW and KRISO 3 MW wind turbines

Title	Units	NREL	KRISO
Gear box ratio	N/A	97:1	90:1
Generator Efficiency	%	94.4	90.6977
Rated Mechanical Power	MW	5.30	3.31
Rated Generated Speed	rad/sec	121.68	160.22
Maximum Generator Torque	N-m	47402.91	22708.95
Rated Wind Speed	m/sec	11.40	11.74
Drivetrain Inertia about LSS	kg-m ²	4.378E+07	1.180E+07
Generator Inertia about LSS	kg-m ²	5.026E+06	6.480E+05
Rotor Inertia about LSS	kg-m ²	3.876E+07	1.116E+07
Blade-Pitch Angle at which the Rotor Power Has Doubled (θ_k)	deg	6.30	2.19

Table 2 Sensitivities of aerodynamic power to blade pitch of NREL 5MW and KRISO 3MW wind turbines

Wind Speed (m/sec)	Pitch Angle (deg)		Sensitivity of power to pitch (watt/rad)	
	NREL	KRISO	NREL	KRISO
	11.40(NREL)/ 11.74(KRISO)-Rated	0	0	-2.824E+7
12	3.83	2.652	-4.373E+7	-7.485E+06
14	8.70	7.679	-5.844E+7	-1.805E+07
16	12.06	11.2	-7.046E+7	-2.377E+07
18	14.92	14.12	-8.394E+7	-2.867E+07
20	17.47	16.72	-9.471E+7	-3.284E+07
22	19.94	19.09	-1.059E+8	-3.728E+07
24	22.35	21.29	-1.202E+8	-4.215E+07

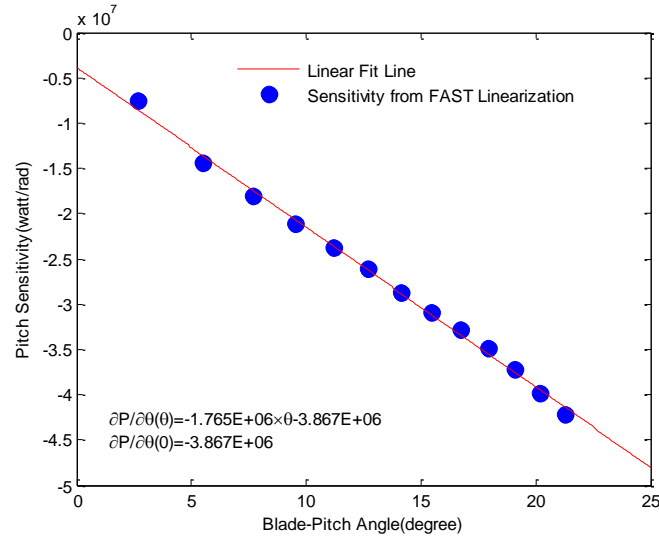


Fig. 2 Pitch sensitivity in relation to blade-pitch angle of KRISO 3 MW wind turbine

3. Numerical simulation in time domain

KRISO FOWT has four wind turbines on a semi-submersible hull. In order to calculate the full coupling dynamics among multiple turbines, mooring lines, and the floater, the aero-rotor-tower CAE program developed by NREL, called FAST (Jonkman and Buhl 2005), was expanded and combined with the floater-mooring coupled dynamic analysis program, CHARM3D (e.g., Kim *et al.* 2001, Tahar and Kim 2003, Yang and Kim 2010). The dynamic responses of the MUFOWT can be obtained from the full DOFs including floater 6-DOFs and additional multi-wind-turbine DOFs with proper platform-turbine coupling terms. The entire MUFOWT-coefficient matrix with forcing functions in the right-hand side was solved simultaneously at each time step. Assuming that the degree of freedom for a three-bladed turbine in FAST is turned on with 19 modes, the total DOFs of MUFOWT can be expressed as $6+19 \times N$, where N is the total number of turbines. The inertia and active forces from each turbine should be independently fed to couple with the sharing floater. The coupled terms between a floating platform and each turbine in the coefficient matrix can be derived by accounting for every effect of inertia and active forces from both bodies. If the blade pitch control is included in the simulation, then additional damping effect is added to the platform motions and aero-dynamic force caused by the blade pitch control is added on the blade, and it also affects the FOWT dynamics. The detailed theory and equation are given in Bae and Kim (2014).

The hydro-dynamic loadings and mooring restoring forces are obtained from CHARM3D, which calculates all of the external forces acting on the floating platform and feeds the external forces to FAST at each time step. The transferred external forces include first-order and second-order wave forces, radiation damping force in terms of convolution integral, nonlinear viscous drag forces at respective instantaneous positions of Morison members, and mooring-induced restoring forces. Then FAST fills out the forcing function of platform DOFs using those transferred forces, and solves displacements, velocities, and accelerations of all

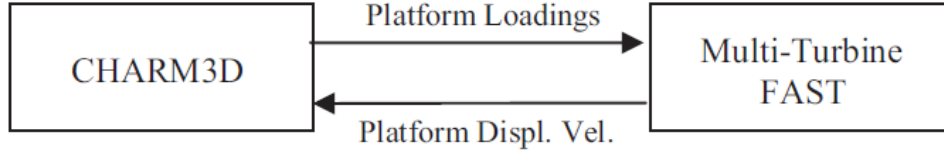


Fig. 3 Basic concept of FAST-CHARM3D coupling

degrees of freedom including elastic responses of towers and blades. The obtained platform kinematic data are then fed into CHARM3D side to update the external forces. The procedure is repeated for the next time step. The basic concept of rotor-floater coupling is schematically shown in Fig. 3. The developed MUFOWT program can be used for single-wind-turbine floating base like OC4-semisubmersible as well as multi-wind-turbine floating base like KRISO semisubmersible.

4. Negative damping caused by thrust force in the pitch motion of offshore wind turbine

The governing equation of platform pitch motion can be expressed as follows

$$(I + I^a(\infty))\ddot{\xi} + \int_{-\infty}^t R(t-\tau)\dot{\xi}(\tau)d\tau + (K_H + K_M)\xi = M_{Diff} + M_{Vis}(\dot{\xi}) + L_H T_w(\dot{\xi}) \quad (10)$$

where I is platform pitch inertia, I^a is added inertia of pitch at infinite wave frequency, R is the retardation function that is Fourier cosine transform of radiation damping, K_H is hydrostatic restoring coefficient, K_M is the mooring related restoring coefficient, M_{Diff} is wave diffraction moment, M_{vis} is the wave induced viscous drag moment, and L_H is hub height and T_w is thrust force at hub. In this equation, the convolution-integral force, viscous-drag moment, and wind-thrust force are the functions of the platform pitch angular velocity, and those terms give damping effect to the platform pitch motion.

In the viscous pitch moment, only the platform pitch angular velocity term can be expressed like Eq. (11), and C_{vis} is given by Morison's equation for the surge and heave directions

$$M_{Vis}(\dot{\xi}) = C_{Vis}\dot{\xi} \quad (11)$$

$$C_{Vis} = \left(\sum_{n=1}^m C_s \int -z^2 |u_{rel} - z\dot{\xi}| dz + \sum_{k=1}^l C_h \int -x^2 |w_{rel} - x\dot{\xi}| dx \right) \quad (12)$$

where C_s and C_h are surge and heave drag coefficients respectively, m and l are the numbers of the surge and heave Morison members, u_{rel} and w_{rel} are the relative velocities between platform surge/heave velocity and surge/heave directional wave particle velocity. C_{vis} is always negative in the right side, thus the pitch damping caused by the fluid-induced viscous force is always positive.

The negative damping can be caused by the aerodynamic rotor thrust force. The aerodynamic rotor thrust depends on the relative speed between translational speed at hub and wind speed, rotor speed, and blade-pitch angle. In order to understand how the thrust sensitivity to the wind speed

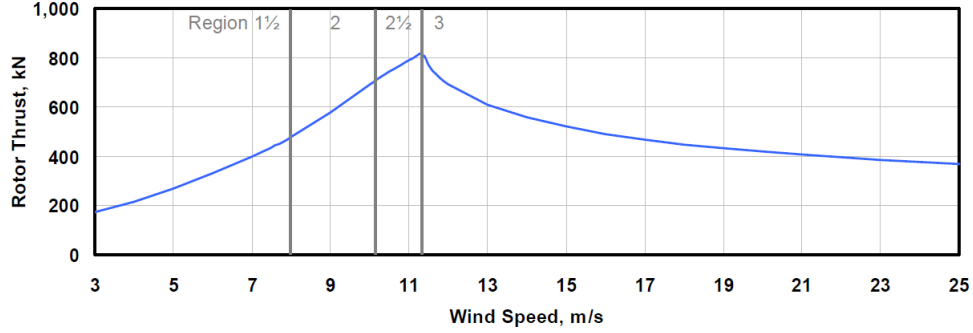


Fig. 4 Steady-state rotor thrust as a function of wind speed for the NREL 5-MW base line wind turbine

affects the platform pitch damping, the thrust force is linearized using the first-order Taylor series expansion (Jonkman 2008, Larsen and Hanson 2007).

$$\Delta T = \frac{\partial T}{\partial(V - \dot{x})} \Delta(V - \dot{x}) + \frac{\partial T}{\partial \beta} \Delta \beta + \frac{\partial T}{\partial \Omega} \Delta \Omega \quad (13)$$

where T is the thrust, \dot{x} is the translational hub speed, V is the wind speed at hub, β is the blade pitch angle, and Ω is the rotor speed. Because the translational hub speed is very small compared to the wind speed, the thrust sensitivity to the relative wind speed can be well represented by the thrust sensitivity to the wind speed.

$$\Delta T = \frac{\partial T}{\partial V} \Delta(V - \dot{x}) + \frac{\partial T}{\partial \beta} \Delta \beta + \frac{\partial T}{\partial \Omega} \Delta \Omega \quad (14)$$

The wind speed term and the hub translational speed term can be divided.

$$\Delta T = \frac{\partial T}{\partial V} \Delta(V - (\dot{X} + L_H \Delta \dot{\xi})) + \frac{\partial T}{\partial \beta} \Delta \beta + \frac{\partial T}{\partial \Omega} \Delta \Omega \quad (15)$$

where \dot{X} is the platform surge velocity. The pitch induced hub translational speed can be estimated by the multiplication of hub height by platform pitch angular speed in case of small pitch angle.

$$\Delta T = \frac{\partial T}{\partial V} \Delta(V - \dot{X}) + \frac{\partial T}{\partial V} (-L_H \Delta \dot{\xi}) + \frac{\partial T}{\partial \beta} \Delta \beta + \frac{\partial T}{\partial \Omega} \Delta \Omega \quad (16)$$

The second term is the function of the angular velocity of platform pitch, thus it directly affects the pitch damping. The second term can be negative damping when the thrust decreases with wind speed. Actually, the thrust is inversely proportional to the wind speed in the range above rated wind speed as shown in Fig. 4, so it may produce negative pitch damping. However, the blade pitch motion is normally slow compared to the changes in wind speed, and the reaction speed of the blade pitch angle to the wind speed can be controlled by changing the natural frequency of blade pitch control. More sensitively the blade pitch angle changes to the wind speed, larger negative pitch damping the platform has. If the BPC natural frequency is small, the blade pitch angle responds slowly even though the wind speed increases, thus thrust will increase according to the wind speed. On the contrary, larger the BPC natural frequency, more likely to have decreasing

thrust as Fig. 4. Therefore, it is better to use small BPC natural frequency to prevent the negative pitch damping in the operational condition.

5. Case study 1. OC4 DeepCwind floating offshore wind-turbine

In order to find the effect of BPC (blade pitch control) on semi-submersible-type FOWT, various simulations are performed with changing natural frequency, damping ratio, and wind speed. As the first example, OC4 semi-submersible FOWT is selected. The detailed descriptions of tower, platform, and mooring system are given in Kim and Kim (2015). The applied environmental conditions are summarized in Table 3. JONSWAP spectrum represented with 100 wave components is used. Randomly perturbed frequency interval is used to warrant non-repetitiveness of signal in 3-hour time histories. We also used 400-second ramping time to minimize transient effects. Before investigating the FOWT case, let us first briefly explain the case of land-fixed case with the same 5 MW wind turbine. NPD wind spectrum is used.

5.1 Thrust force of on-land wind turbine with various natural frequencies and damping ratios

Before investigating the effect of BPC on floating wind turbines, let us first consider the case of land-fixed wind turbine. This is helpful to understand how the thrust force changes according to various wind speeds and BPCNFs without considering floater motions. In the case of on-land wind turbine, it is assumed that the same 5-MW wind turbine as that used in the OC4-FOWT is installed as a cantilever beam to the ground. If the wind turbine is fixed with the average wind speed of 8 m/sec, the blade pitch control is not necessary because the maximum wind speed is less than the rated wind speed (11.4 m/s). In this case, the thrust force spectrum has almost the same shape as the wind spectrum, as shown in Fig. 5. Blade pitch control works in the higher wind speed than the rated wind speed. Then, the additional thrust force is generated near the damped natural frequency of the blade pitch control. As the natural frequency of blade-pitch control increases, the amplitude of additional thrust becomes larger, as shown in Fig. 6. In Fig. 7, we show the effect of various wind speeds while fixing the blade-control natural frequency and damping ratio.

Table 3 environmental condition used in case study for OC4 DeepCWind semi-submersible FOWT

Wave	Significant height(m)	7.17
	Peak frequency(rad/sec)	12.1
	Gamma	2.2
	Heading(deg)	0
	Spectrum	JONSWAP wave spectrum
Wind	Speed at hub(m/s)	0 m/sec, 8 m/sec, 11.4 m/sec, 14.5 m/sec, 16 m/sec, 19 m/sec, 22 m/sec
	Spectrum	NPD wind spectrum
Current	Speed(m/s)	0

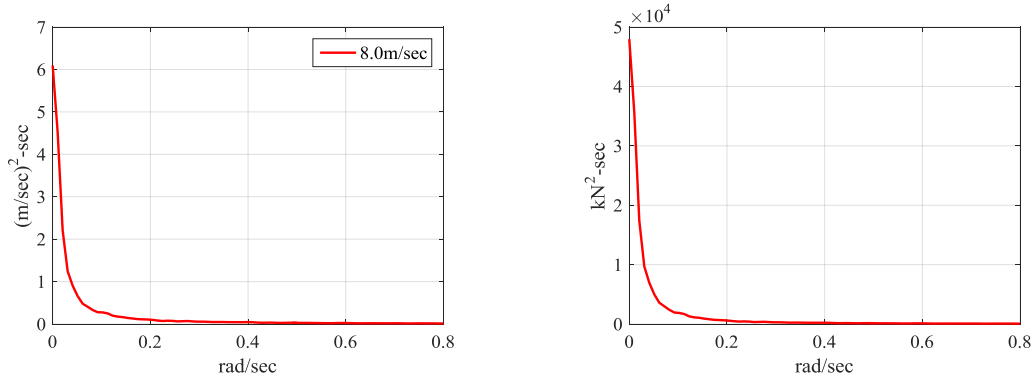


Fig. 5 8 m/sec wind speed PSD (left) and thrust force PSD (right) of on-land turbine without blade pitch control

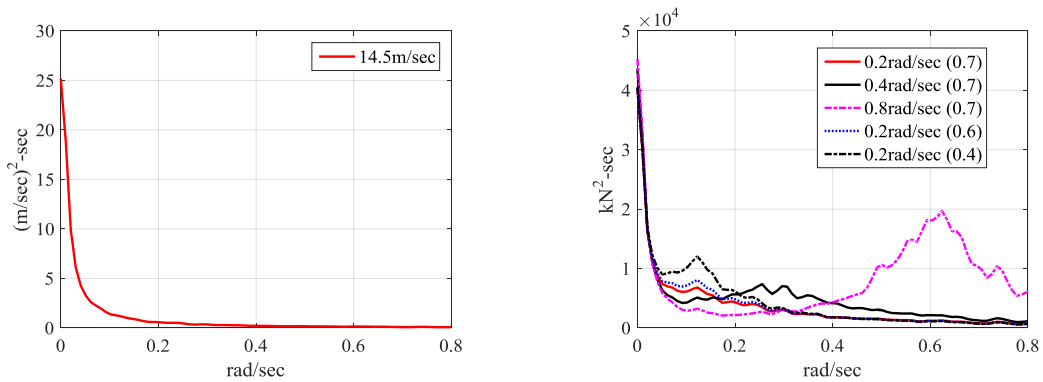


Fig. 6 NPD wind spectrum (left) with 14.5 m/sec averaged wind speed and thrust force PSD (right) of on-land wind turbine for various blade pitch control natural frequencies and damping ratios. (The values in parentheses=the damping ratio)

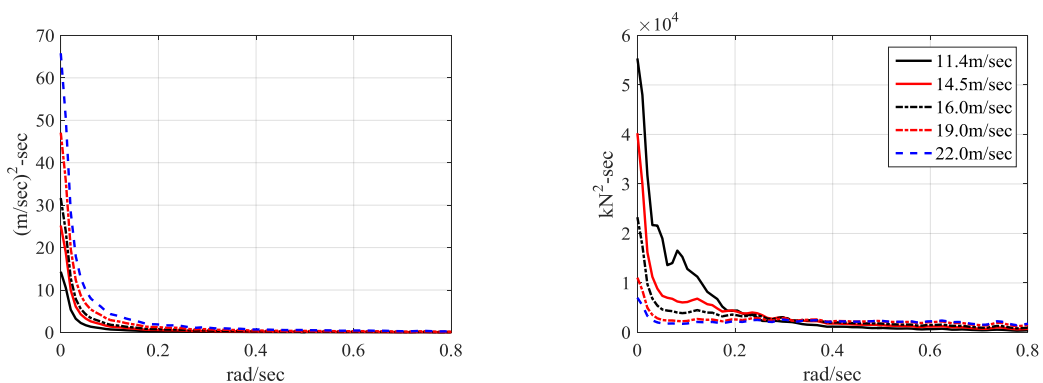


Fig. 7 Wind speed PSD (left) and thrust PSD (right) for on-land wind turbine in various wind speeds when natural frequency is 0.2 rad/sec and damping ratio is 0.7

It shows that the thrust decreases in the low frequency region less than 0.3 rad/sec as the average wind speed increases due to the BPC. This result matches with Fig. 4, in which the thrust force decreases as the wind speed increases in the wind-speed region higher than the rated wind speed. In summary, in case of land-fixed wind turbine, there may be appreciable increase of thrust when BPCNF becomes higher. As BPCDR becomes lower, the thrust tends to increase.

5.2 Effects of BPC on platform thrusts and pitch motions

Next, DeepCWind semi-submersible FOWT is considered. The detailed description of the system and the global-performance simulations compared with experiments are summarized in Kim *et al.* (2017). The numerical results agreed well with the experimental results. In this paper, we focus on the effects of BPCNF and BPCDR on platform pitch motions, thrust, and the generated power quality. The platform pitch natural frequency without wind damping is 0.23 rad/s. With additional wind damping, it is to be slightly reduced. In Fig. 8, the thrust spectral amplitudes and platform-pitch spectral amplitudes are plotted with increasing wind speeds for the fixed BPCNF=0.2 rad/s and BPCDR=0.7. The thrusts follow the previously observed trends i.e. initially increasing with wind speed up to the rated wind speed, then starting to decrease as wind speed further increases. In the high frequency region between 0.6 and 0.8 rad/s, the thrusts, although they are relatively small, continue to increase with wind speeds. On the other hand, for platform pitch motions, we see significant variations of peak amplitudes with wind speeds near the platform-pitch natural frequency (0.23 rad/s). The peak amplitudes initially decrease with wind speed when wind speed is below the rated wind velocity. It is due to the greatly increased wind-induced pitch damping since large relative blade angles to wind is maintained to have maximum power in that region. When wind speed becomes greater than the rated wind velocity, the relative blade angles get reduced to reduce the thrust. As a result, the wind-induced pitch damping becomes smaller and the peak amplitudes become increased. At the highest wind speed 19m/s, the blade angles are so small that the resulting wind-induced pitch damping becomes minimal. So, the corresponding pitch motions near the platform-pitch natural frequency are similar to those of no-wind case. In Fig. 8, although the BPCNF is given as 0.2, the actual damped BPCNF changes according to the blade pitch angle (or wind speed) based on Eqs. (1)-(9). The corresponding maximum and minimum blade pitch angles and damped BPCNFs for various wind speeds are tabulated in Table 4.

Table 4 Maximum, minimum, and mean blade pitch angles and damped natural frequencies of blade pitch control in various wind speeds when its natural frequency is 0.2 and damping ratio is 0.7 in zero blade pitch angle

Wind Speed (m/sec)	Blade Pitch Angle (deg)			Damped Natural Frequency (rad/sec)		
	Max	Min	Mean	Max	Min	Mean
8.0	0.00	0.00	0.00	0.143	0.143	0.143
11.4	7.79	0.00	1.53	0.118	0.143	0.140
14.5	13.57	1.75	9.32	0.104	0.139	0.114
19.0	20.02	11.04	16.36	0.092	0.109	0.098

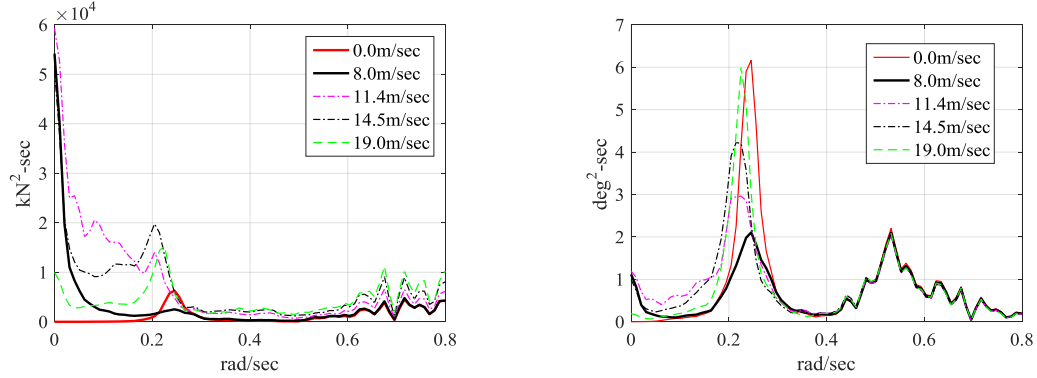


Fig. 8 Thrust force PSD (left) and platform pitch PSD (right) in various wind speeds when the natural frequency of blade pitch control is 0.2 and its damping ratio is 0.7

Table 5 Statistics of thrust forces at hub and platform pitch responses in various wind speeds when the natural frequency of blade pitch control is 0.2 and its damping ratio is 0.7

	Wind Speed (m/sec)	Max	Min	Mean	Std
Thrust Force (kN)	11.4	278.5	-83.0	92.6	43.2
	14.5	737.5	298.1	496.8	56.0
	16.0	1039.6	477.4	800.4	83.6
	19.0	1003.3	279.1	584.8	82.1
	22.0	787.8	171.8	461.1	74.7
Platform Pitch (deg)	11.4	2.899	-3.282	-0.056	0.813
	14.5	4.303	-1.491	1.772	0.717
	16.0	5.812	-0.202	3.155	0.815
	19.0	4.843	-1.113	2.191	0.826
	22.0	4.393	-1.399	1.655	0.818

5.3 Effects of BPCNF on platform pitch motions and generated power

Fig. 9 shows the platform pitch and thrust PSDs for various BPCNFs when BPCDR=0.7 and average wind velocity=14.5 m/s (above rated wind velocity=11.4 m/s). We can see that the resonance peak amplitudes of platform pitch continue to increase as BPCNF increases until 0.8 rad/s. This is due to the reduction of platform-pitch damping caused by negative damping associated with the BPC. After 0.8 rad/s, the peak drops. Similar to Fig. 6, thrusts increase significantly in 0.6~1 rad/s when BPCNF is above 0.8 rad/sec. Fig. 10 shows the time histories and spectra of the generated power. When BPCNF is higher than 0.8 rad/s, we start to see appreciable

fluctuations in the high-frequency region. Again, the generated power quality is the best with minimal fluctuations when BPCNF=0.2~0.3rad/s i.e., BPCNF is slightly lower or slightly higher than the platform pitch natural frequency (0.23 rad/s). The related statistics of the platform pitch motions and thrusts are given in Table 6.

5.4 Effects of BPCDR on platform pitch motions and generated power

In the previous example, we have seen the best performance when BPCNF=0.2. So, in this section, we fix BPCNF=0.2 and check the sensitivity against various BPCDRs for the given average wind speed=14.5 m/s.

Table 6 Statistics of platform pitch and thrust force at hub in natural frequency when the wind speed is 14.5 m/sec and radiation damping is 0

	Natural Frequency (rad/sec)	Max	Min	Mean	Std
Platform Pitch (deg)	0.2	4.843	-1.113	2.191	0.826
	0.3	6.571	-2.171	2.199	0.986
	0.4	7.495	-2.532	2.210	1.428
	0.8	9.565	-4.254	2.239	1.997
	1.0	9.323	-4.387	2.247	1.582
Thrust Force (kW)	0.2	5837.5	4279.2	4999.2	236.1
	0.3	5754.7	2896.8	4998.5	203.7
	0.4	5726.9	2769.7	4995.3	218.2
	0.8	5518.6	3233.8	4986.3	180.6
	1.0	5611.9	3321.9	4982.4	195.7

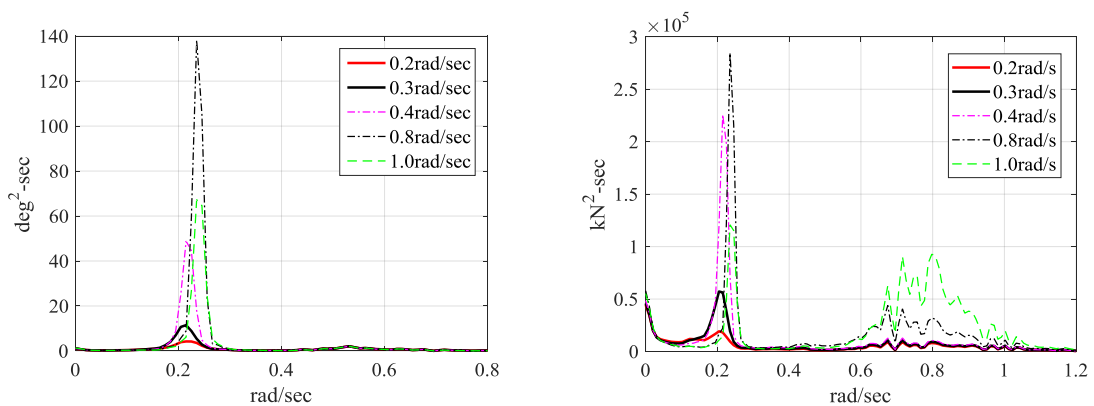


Fig. 9 Platform pitch PSD (left) and thrust PSD (right) for various BPCNFs when damping ratio is 0.7 and average wind speed is 14.5 m/sec

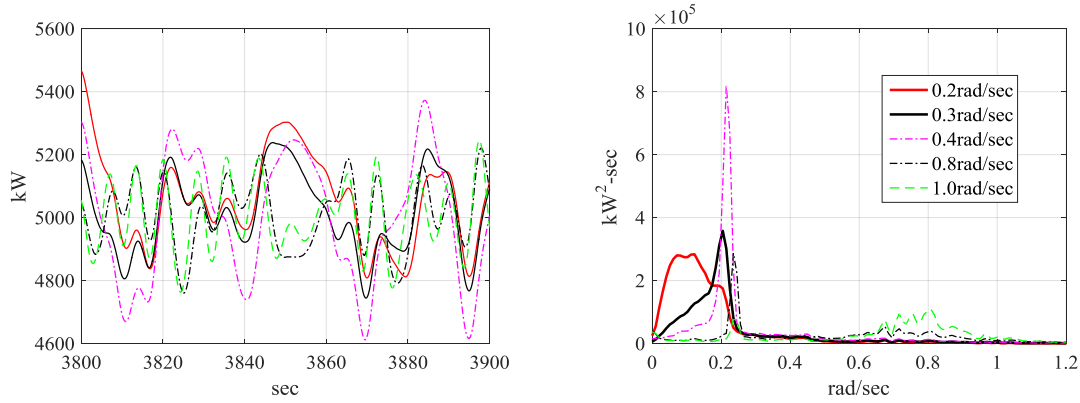


Fig. 10 Generated power time series and PSD in various natural frequencies when damping ratio is 0.7 and average wind speed is 14.5 m/sec

Fig. 11(a) shows the platform-pitch PSDs for various BPCDRs. Below the BPCNF, the platform-pitch spectral amplitudes become smaller with higher BPCDR. However, near the platform-pitch natural frequency, the opposite trend can be found i.e., the peak amplitudes increase with BPCDR. Therefore, those two effects compensate to each other. Other than those two regions, the spectral amplitudes do not change with different BPCDR since damping typically only affects the resonance region. Fig. 11(b) shows the corresponding generated-power PSDs. We see that higher BPCDR results in less fluctuation in the generated power. Overall, the BPCDR=0.7 gives us the best performance. The related statistics of the platform pitch motions and generated power outputs are given in Table 7. So far, we can conclude that in the BPC region above rated wind velocity, BPCDR=0.7 and BPCNF=0.2 (slightly less than platform pitch natural frequency) produced the best BPC performance.

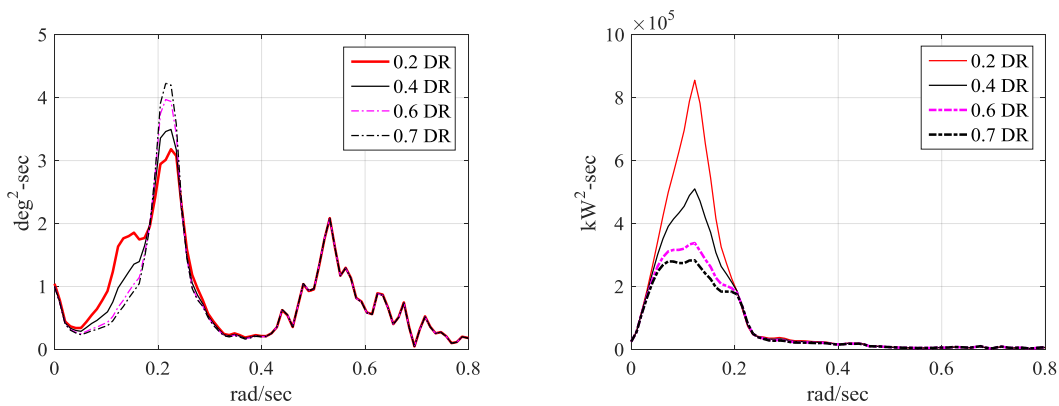


Fig. 11 Platform pitch PSD (left) and generated power PSD (right) in various damping ratio when natural frequency is 0.2

Table 7 Statistics of platform pitch and generated power in various damping ratio when the wind speed is 14.5 m/sec and natural frequency is 0.2 rad/sec

	Damping Ratio	Max	Min	Mean	Std
Platform Pitch (deg)	0.2	5.310	-1.023	2.194	0.856
	0.4	4.964	-0.810	2.192	0.833
	0.6	4.875	-1.032	2.191	0.826
	0.7	4.843	-1.113	2.191	0.826
Power (kW)	0.2	6223.6	3976.2	4999.4	319.0
	0.4	6025.0	4123.1	4999.3	277.2
	0.6	5890.8	4233.1	4999.2	247.9
	0.7	5837.5	4279.2	4999.2	236.1

5.5 Effect of wind-speed change on platform pitch motions and generated power with fixed BPCNF and BPCDR

In this section, wind speed is varied from 11.4 m/sec to 22.0 m/sec while fixing BPCNF= 0.2 and BPCDR=0.7. As wind speed increases, the platform-pitch resonance peaks increase due to the reduced wind-induced damping as a result of using smaller blade angles. However, the opposite trend holds true in the low frequency region below 0.2 rad/s due to the decreasing wind-induced slowly-varying thrusts with higher wind speeds after the rated wind velocity (11.4 rad/s). We also employed in Fig. 12(b) another case of BPCNF=0.6 for comparison. In this case, we observe the effect of BPC-induced negative damping in pitch motion and the resulting platform-pitch amplitudes are greatly amplified by resonance, In particular, we have the largest amplification when wind speed=14.5 m/sec. In very high wind speeds above 19 m/sec, the negative damping effect becomes much smaller than that in lower wind speed, as shown in Table 8 and Fig. 12. In summary, significantly increased platform-pitch motions may happen when BPCNF is higher than platform-pitch natural frequency, which should be avoided in FOWT design.

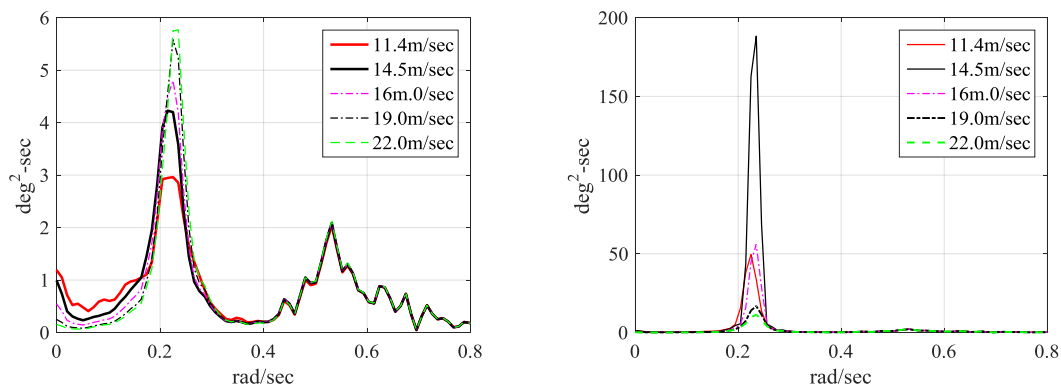


Fig. 12 Platform pitch time series and PSD in various wind speed when damping ratio is 0.7 and the natural frequency is 0.2 rad/sec (left) when damping ratio is 0.7 and the natural frequency is 0.6 rad/sec (right) in zero blade pitch angle

Table 8 Statistics of platform pitch in various wind speed when the damping ratio is 0.7 and natural frequency is 0.6 rad/sec and 0.2 rad/sec

	Damping Ratio	Natural Frequency (rad/sec)	Wind Speed (m/sec)	Max	Min	Mean	Std
Platform Pitch (deg)	0.7	0.6	11.4	8.244	-3.483	3.127	1.464
			14.5	9.271	-4.664	2.238	2.321
			16	8.121	-3.416	1.975	1.44
		19	5.848	-1.881	1.676	1.008	
		22	4.902	-1.729	1.495	0.922	
		11.4	5.812	-0.202	3.155	0.815	
	0.2	0.6	14.5	4.843	-1.113	2.191	0.826
			16	4.547	-1.401	1.955	0.819
			19	4.393	-1.687	1.668	0.82
		22	4.265	-1.789	1.488	0.822	

6. Case study 2. KRISO multi-unit floating offshore wind-turbine

KRISO-MUFOWT is also employed as the second example of sensitivity investigation regarding BPCNF and BPCDR for platform pitch motions. There are four 3MW wind turbines at the corners of square-type semi-submersible hull. The detailed description of this case is given in Kim *et al.* (2017). In the same paper, the numerical simulations for various cases were well verified against KRISO experimental results. For simplicity, the wind-wake effects for downstream turbines are not considered. The fully-coupled simulation of the entire system was done by using the same numerical tool developed by Bae and Kim (2014). In this case, the platform pitch natural frequency is 0.4 rad/s and rated wind velocity is 11.7 m/s. The cases and environmental conditions used for the simulations are tabulated in Tables 9 and 10. The applied wind speed is 13 m/s (above rated wind velocity 11.7 m/s). NPD wind spectrum is used.

6.1 BPCDR sensitivity test

First of all, the BPCDR sensitivity test was performed. The simulation time is 2000sec. The BPCNF was fixed at 0.3 rad/sec (below platform-pitch natural frequency=0.4 rad/s) and BPCDR was varied from 0.2 to 0.8. The time histories and spectra of generated power, blade angle, platform-surge and pitch motions are given in Figs. 13-16. We can see that platform surge and pitch motions are minimally affected by the change of BPCDR. If BPCDR increases, the generated power is more regulated with less fluctuation. If BPCDR is greater than 0.65, there is little change in the quality of the generated power. This conclusion is consistent with that drawn from the OC4-5 MW-submersible case.

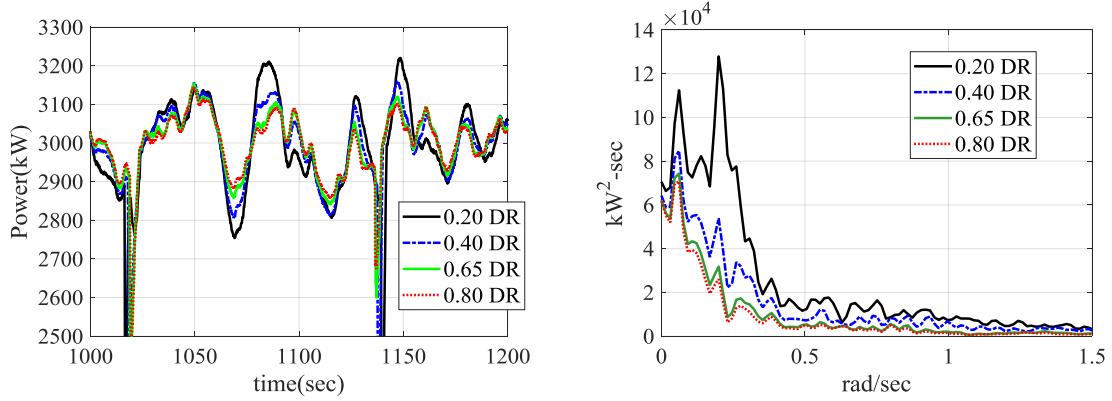


Fig. 13 Generated Power time series (left) and power spectrum density (right) in BPCDR test

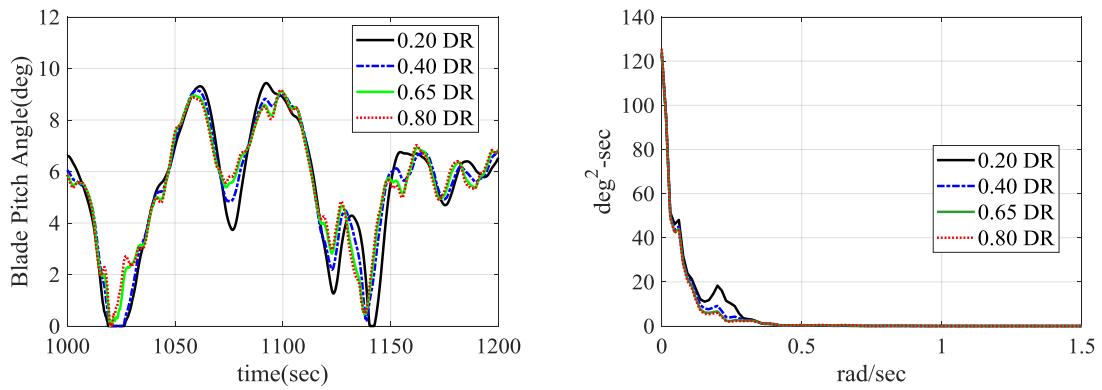


Fig. 14 Blade pitch angle time series (left) and power spectrum density (right) in BPCDR test

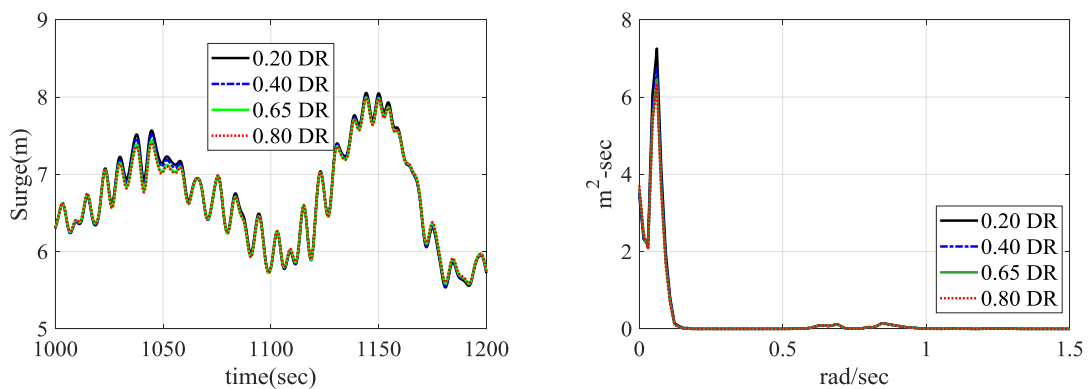


Fig. 15 Platform surge motion time series (left) and power spectrum density (right) in BPCDR test

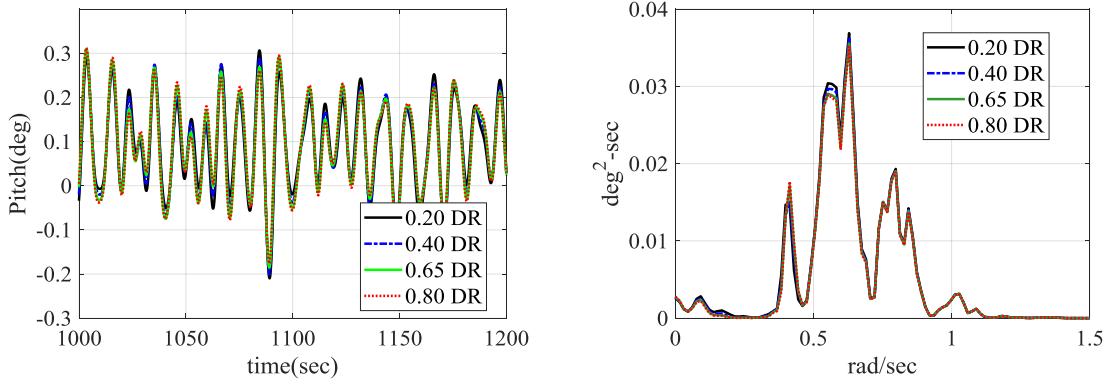


Fig. 16 Platform pitch motion time series (left) and power spectrum density (right) in BPCDR test

Table 9 Cases used in BPCDR sensitivity

	1	2	3	4
BPCNF(rad/sec)			0.3	
BPCDR	0.2	0.4	0.65	0.8

Table 10 Environmental condition used in BPCDR sensitivity

Wave	Significant height(m)	3.38
	Peak frequency(rad/sec)	0.74
	Gamma	2.2
	Heading(deg)	0
Wind	Speed at hub(m/s)	13
	Turbulence intensity (%)	10
Current	Speed(m/s)	0

6.2 BPCNF sensitivity test

Second, the BPCNF sensitivity test was conducted for fixed BPCDR=0.65. The simulation time is 2000sec. Four BPCNFs were selected, 0.2, 0.3, 0.41, and 0.74 rad/sec. 0.41 rad/s is very close to platform-pitch natural frequency and 0.74 rad/sec is the wave peak frequency. The time histories and spectra of generated power, blade angle, platform-surge and pitch motions are given in Fig. 17-20. We can see that platform surge motions are minimally affected by the change of BPCDR. When we examine the platform-pitch resonance peaks, as observed before, their amplitudes increase with increasing BPCNF up to 0.74 rad/s. After that, there is slight drop. Other frequency regions are minimally influenced by the change of BPCNF. Overall, the influence on platform-pitch motions by BPC is less compared to the previous case due to smaller-size turbines

and their effects are mingled and not all in phase. When BPCNF is significantly lower than platform-pitch natural frequency, like 0.2 rad/s case, the quality of generated power becomes worsened, as can be seen in Fig. 17. However, the differences become small after 0.3 rad/s. Therefore, increasing BPCNF causes larger platform-pitch resonance peaks. On the other hand, significantly lowering BPCNF causes more fluctuations in the generated power. So, the range 0.3~0.4 rad/s appears to be optimal. Again, “slightly less than the platform-pitch natural frequency” is the best.

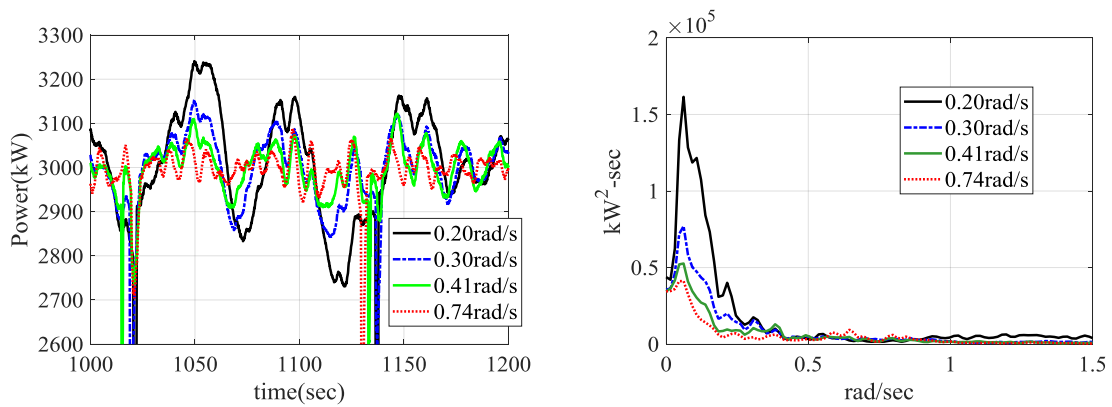


Fig. 17 Generated Power time series (left) and power spectrum density (right) in BPCNF test

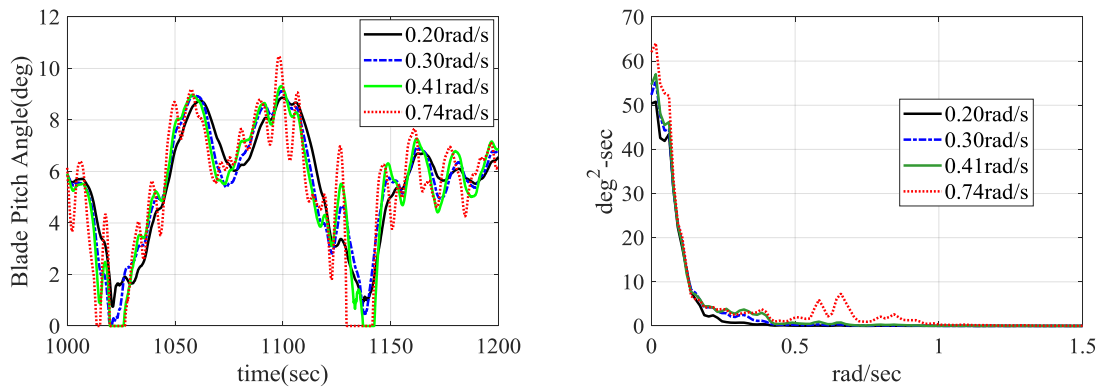


Fig. 18 Blade pitch angle time series (left) and power spectrum density (right) in BPCNF test

Table 11 Cases used in BPCNF sensitivity

	1	2	3	4
BPCNF(rad/sec)	0.2	0.3	0.41	0.74
BPCDR		0.65		

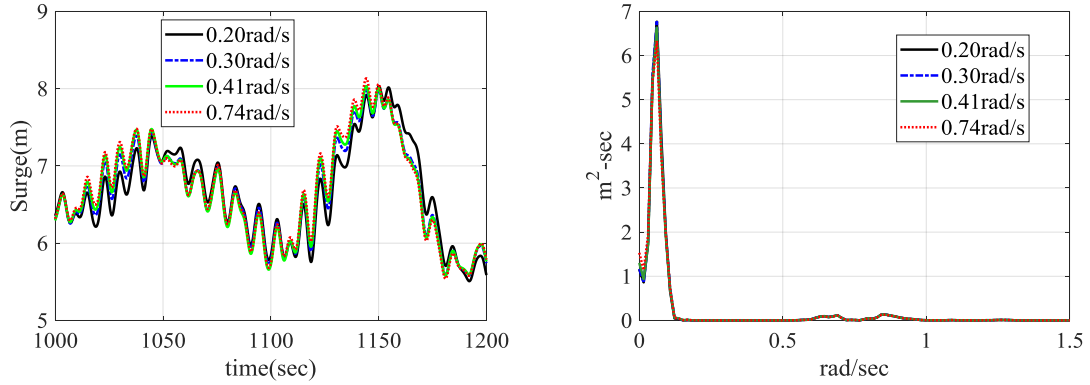


Fig. 19 Platform surge motion time series (left) and power spectrum density (right) in BPCNF test

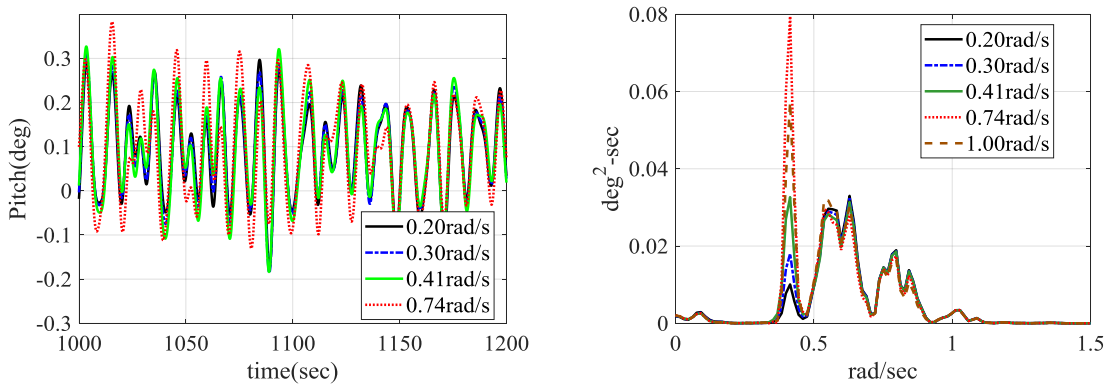


Fig. 20 Platform pitch motion time series (left) and power spectrum density (right) in BPCNF test

7. Conclusions

In this paper, in order to find the effect of BPC on floating-platform motions and generated power, fully-coupled computer simulation programs are used to study two cases, OC4-5MW semi-submersible FOWT and KRISO 4-3 MW-units FOWT. Various simulations are performed changing BPC natural frequency, BPC damping ratio, and wind speeds. Through the numerical simulations, it was demonstrated that negative damping can happen for platform pitch motions and its influences are affected by BPCNF, BPCDR, and wind speeds. In both examples, it was found that BPCDR range of 0.6~0.7 gives the best quality of generated power. If BPCNF is significantly larger than platform-pitch natural frequency, the pitch resonance can be very serious due to the BPC-induced negative-damping effects, which should be avoided in the FOWT design. When BPCNF is slightly smaller (or slightly higher) than platform-pitch natural frequency, both pitch motions and generated power become optimal. If BPCNF is significantly lower than platform-pitch natural frequency, the fluctuations in the generated power are increased. BPC negative-damping can only happen at wind speeds higher than the rated wind velocity. If wind

speed is significantly higher than the rated wind velocity, the negative damping effects start to become reduced.

References

- Bae, Y.H. and Kim, M.H. (2011), "Rotor-floater-mooring coupled dynamic analysis of mono-column-TLP-type FOWT (Floating Offshore Wind Turbine)", *Ocean Syst. Eng.*, **1**(1), 95-111.
- Bae, Y.H. and Kim, M.H. (2014), "Coupled dynamic analysis of multiple wind turbines on a large single floater", *Ocean Eng.*, **92**, 175-187.
- Hansen, M., Hansen, A., Larsen, T., Øye, S., Sørensen, P. and Fuglsang, P. (2005), Control Design for a Pitch-Regulated. Variable Speed Wind Turbine.
- Jonkman, J. (2008), "Influence of control on the pitch damping of a floating wind turbine", Paper presented at the 46th AIAA Aerospace Sciences Meeting and Exhibit.
- Jonkman, J. (2010), Definition of the Floating System for Phase IV of OC3. Retrieved from
- Jonkman, J. M. and Buhl Jr, M. L. (2005). Fast user's guide-updated august 2005. Retrieved from
- Jonkman, J., Butterfield, S., Musial, W. and Scott, G. (2009), Definition of a 5-MW reference wind turbine for offshore system development, Retrieved from
- Kim, H.C. and Kim, M.H. (2015), "Global performances of a semi-submersible 5 MW wind-turbine including second-order wave-diffraction effects", *Ocean Syst. Eng.*, **5**(3), 139-160.
- Kim, H.C. and Kim, M.H. (2016), "Comparison of simulated platform dynamics in steady/dynamic winds and irregular waves for OC4 semi-submersible 5MW wind-turbine against DeepCwind model-test results", *Ocean Syst. Eng.*, **6**(1), 1-21.
- Kim, H.C., Kim, K.H., Kim, M.H. and Hong, K. (2017), "Global performance of a KRISO semisubmersible multiunit floating offshore wind turbine: Numerical simulation vs. model test", *Int. J. Offshore Polar Eng.*, **27**(1), 70-81.
- Kim, M.H. and Yue, D.K. (1989), "The complete second-order diffraction solution for an axisymmetric body Part 1. Monochromatic incident waves", *J. Fluid Mech.*, **200**, 235-264.
- Kim, M.H. and Yue, D.K. (1990), "The complete second-order diffraction solution for an axisymmetric body Part 2. Bichromatic incident waves and body motions", *J. Fluid Mech.*, **211**, 557-593.
- Kim, M.H. and Yue, D.K. (1991), Sum and difference-frequency wave loads on a body in unidirectional Gaussian seas.
- Kim, M.H., Ran, Z. and Zheng, W. (2001), "Hull/mooring coupled dynamic analysis of a truss spar in time domain", *Int. J. Offshore Polar Eng.*, **11**(1).
- Larsen, T.J. and Hanson, T.D. (2007), "A method to avoid negative damped low frequent tower vibrations for a floating, pitch controlled wind turbine", Paper presented at the Journal of Physics: Conference Series.
- Namik, H. and Stol, K. (2011), "Performance analysis of individual blade pitch control of offshore wind turbines on two floating platforms", *Mechatronics*, **21**(4), 691-703.
- Tahar, A. and Kim, M.H. (2003), "Hull/mooring/riser coupled dynamic analysis and sensitivity study of a tanker-based FPSO", *Appl. Ocean Res.*, **25**(6), 367-382.
- Yang, C.K. and Kim, M.H. (2010), "Transient effects of tendon disconnection of a TLP by hull-tendon-riser coupled dynamic analysis", *Ocean Eng.*, **37**(8-9), 667-677.
- Yang, C.K. and Kim, M.H. (2011), "The structural safety assessment of a tie-down system on a tension leg platform during hurricane events", *Ocean Syst. Eng.*, **1**(4), 263-283.